R. H. Kidd
R. H. Wolfe

Performance Modeling of Earth Resources Remote Sensors

Abstract: A technique is presented for constructing a mathematical model of an Earth resources remote sensor. The technique combines established models of electronic and optical components with formulated models of scan and vibration effects, and it includes a model of the radiation effects of the Earth's atmosphere. The resulting composite model is useful for predicting in-flight sensor performance, and a descriptive set of performance parameters is derived in terms of the model. A method is outlined for validating the model for each sensor of interest. The validation for one airborne infrared scanning system is accomplished in part by a satisfactory comparison of predicted response with laboratory data for that sensor.

Introduction

Multispectral scanning systems are used to gather remotely sensed radiometric data for a wide variety of applications, e.g., pollution monitoring, geological and urban surveying, and crop classification [1–3]. The measure of performance of such a system can be expressed in terms of its image-resolving capability and its radiometric accuracy. The former measures the system's capability to discern a scene from imposed noise, and the latter expresses the accuracy to which the system measures the radiant power from the scene. These performance parameters are critical in assessing the usefulness of a particular system for a particular remote sensing program, and they are instrumental in determining the design requirements of an advanced sensor system.

The desired performance parameters are generally not measured directly, and they must be inferred by mathematical analysis from more direct laboratory measurements and manufacturer's specifications. Such a performance evaluation of existing systems or the development of design requirements for an advanced system can be carried out in a systematic way by constructing a mathematical model of the sensor system, component by component, where each component model is parametrized by performance values obtainable from laboratory measurements or design specifications. The purpose of this paper is to develop a linear systems approach to mathematically model a typical remote sensor configuration and to predict system performance characteristics. This approach, which treats the remote sensor as a communication system, has been used extensively to model electronic systems, as described by Papoulis [4]. The theory has been extended to optical imaging systems by Goodman [5]. Thus, this paper applies the combined optical and electronic systems theories to provide an end-to-end model of the sensor system. In addition to the sensor component characteristics, atmospheric effects are considered.

The discussion is opened with a description of the sensor configuration to be modeled. Next, the mathematical models of the atmosphere and individual system components are developed, and these models are combined to provide the total system model. The components are assumed to be linear, invariant systems, and their models are expressed in terms of transfer functions. The prediction of overall system capability is derived in terms of the transfer functions and system noise characteristics. Finally, the procedure for validating the model with test data is outlined and applied to available laboratory tests for an infrared sensor used in the NASA Earth resources aircraft program.

Typical sensor system

The sensor system considered measures, in a number of spectral bands, the solar radiation reflected from or the thermal radiation emitted by the ground. The general spectral characteristics of the received radiation are illustrated in Fig. 1 for an orbital sensor viewing 300-K ground with 20 percent reflectivity [6]. These characteristics are representative of airborne sensors as well. Typically, a number of narrow spectral bands are utilized in the 0.4 μm to 2 μm wavelength region (from ultraviolet, through visible, to near infrared, respectively), and one or two bands are defined for the thermal infrared region from 8 μm to 14 μm, as shown in Fig. 1.

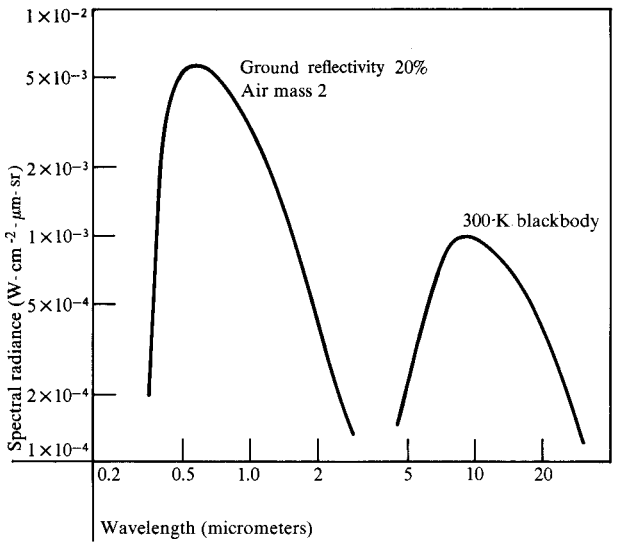

Figure 1 Representative spectrum of ground radiance at sensor incidence for a ground temperature of 300 K and reflectance of 20 percent [6].

The remote sensing system is illustrated by the block diagram in Fig. 2. Light from the ground scene is attenuated and supplemented by the atmosphere before entering the sensor system. A rotating mirror scans the ground perpendicular to the line of flight. The light is reflected by the rotating mirror through the optics and focused on the detector where it is converted to an electrical signal. As the mirror rotates past the calibration sources, their radiation replaces the ground radiation. The detector output is processed electronically and recorded for later image reconstruction. Each of the system elements is described briefly in the following paragraphs.

• *Ground scene*

The ground scene is characterized by the spatial variation of the reflectance, the temperature, or the emissivity; and the departing sensor-bound radiation is dependent upon those quantities. It is the ultimate purpose of remote sensing to reconstruct the ground scene characteristics, and a measure of the system quality is the degree to which the reconstructed image matches the ground scene. Typical scenes of interest include rectangular fields in an agricultural area, thermal variations in a river or bay, and emissivity variations in the ocean.

• *Atmosphere*

The radiant energy received by the optical system of the sensor is the sum of 1) radiant energy from the viewed ground scene transmitted through the atmosphere, 2) radiant energy reflected or emitted by the background and scattered by the atmosphere (Rayleigh scattering and scattering by aerosols, dust and clouds), and 3) radiant solar energy scattered or absorbed by the atmosphere before it reaches the ground. The atmospheric model must account for these three contributions based upon the radiative transfer between the radiation source (the ground scene) and the sensor aperture. Another aspect of atmospheric behavior is the effect of turbulence, which produces a blurring effect in the image, as is well known for images of starlight obtained with telescopes.

• *Scanning mechanism*

A small segment of the ground is viewed at any instant, and the total scene is viewed by scanning by one of several options. A rotating mirror may be situated in front of the primary optics, causing the ground image to sweep along the image plane where the detector is fixed. Or, the detector may be swept along the image plane to scan the scene. The action of the scanning mechanism, in conjunction with the detector, is to convert the spatially varying scene radiance into a temporally varying electrical signal. For airborne sensors, the ground may be scanned a considerable angular displacement to either side of the nadir, and the resulting scene foreshortening is significant in degrading the resolution. Airborne sensors typically use rotating mirrors; spaceborne sensors use other methods because of the high scanning rates required. For example, the Landsat uses an oscillating mirror. Variations in the angular rate of the mirror distort the image and degrade the scene resolution.

• *Optical system*

The optical system essentially amplifies the radiant signal by its light gathering power and produces an image upon the detector. Characteristically, reflection optics are used to maximize the transmitted radiance. Even if the system is aberration free, the limited resolving power (characterized by the optical transfer function discussed subsequently) results in a slightly degraded image definition, and the additional degradation of focus error also merits consideration.

• *Calibration system*

In-flight calibration sources are used as standard references to eliminate the effects of variable sensor gain and bias. The scene radiance is determined directly by comparing the sensor electronic scene response to the corresponding response to the standard sources. In some sensor systems this comparison is provided in flight by use of an automatic gain control keyed to the calibration source response; other sensors leave this task to ground-based processing software.

• *Detector system*

A small detector in the image plane converts the focused radiance into an electrical signal. The portion of the

scene image viewed at any instant by the detector defines the instantaneous field of view (IFOV). The detector is incapable of resolving the image into elements any smaller than its own size, and the resulting spatial averaging over the IFOV causes an additional degradation in resolution. As an electronic system, the detector exhibits certain temporal response characteristics. An effective "shot" noise is created at the detector by the energy fluctuations caused by photon quantization. This noise source is significant in non-thermal spectral bands. Thermal noise is also generated by the detector and is the dominating noise source in the thermal bands. Some detectors that are typically used in the different bands are as follows [7]:

Band	*Detector*
0.4 – 1.0 μm	Photomultiplier tube
	Si photodiode
1.0 – 3.5 μm	InAs photodiode, photovoltaic
1.0 – 5.5 μm	InSb photodiode, photovoltaic, photoconductive
4.0 – 15 μm	HgCdTe photovoltaic. photoconductive

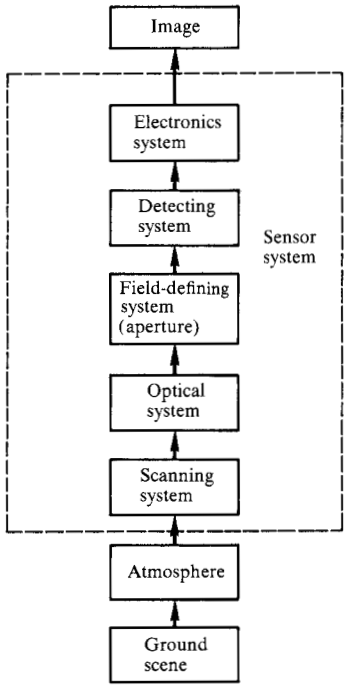

Figure 2 Block diagram of a typical remote Earth resources sensor system.

• *Electronics*

The electronics may consist of preamplifiers, filters, amplifiers, and analog-to-digital converters, as applicable. Each component exhibits a temporal response, characterized by its frequency response function, which further degrades the image definition, now in the form of a time signal. The frequency responses of the preamplifier and filters are generally chosen to minimize detector noise, somewhat at the expense of resolution.

Sensor mathematical model

Linear systems theory is used to characterize the system model. The assumed scene models are expressed in terms of their Fourier components. Each component is modeled by a transfer function (the Fourier transform of the impulse response function for temporal components or of the point spread function for spatial components). The scene signal is passed through the system by multiplying each Fourier component by the transfer function at the corresponding spatial or temporal frequency. The system response is then synthesized from the resulting Fourier components. For the sake of clarity, the system response to a uniform scene (i.e., gain and offset effects only) is handled separately, and the transfer functions are normalized to unity at some frequency (usually zero). The assumption of a linear invariant system is not strictly valid, as shown in later sections of this discussion; the impulse response function is dependent upon the scan angle from nadir and thus is not spatially or temporally invariant. This problem is circumvented by assuming that the changes in the scan angle are small; therefore the response function is approximately invariant. The individual models are treated in the following paragraphs.

• *Ground scene models*

Models for the ground reflectivity or emissivity have been selected to represent realistic conditions, yet be amenable to Fourier analysis. Thus, the reflectance/emittance models chosen are 1) a set of sinusoidal variations of different frequencies, 2) a square wave, and 3) a step change approximated as a segment of a very long period square wave. The ground temperature is not varied in the same way, because ground radiance is not linearly related to temperature and Fourier techniques are not applicable in that case. Thus, a constant reference temperature is selected and the desired temperature variations are approximated by emissivity variations, a method sufficiently accurate for the temperature ranges generally of interest. Emissivity is assumed to be zero for the ultraviolet, visible, and near infrared spectral regions, and reflectivity is assumed to be zero for the thermal bands.

• *Atmosphere models*

The atmospheric scattering, absorption, and emission of radiation are described by the integro-differential

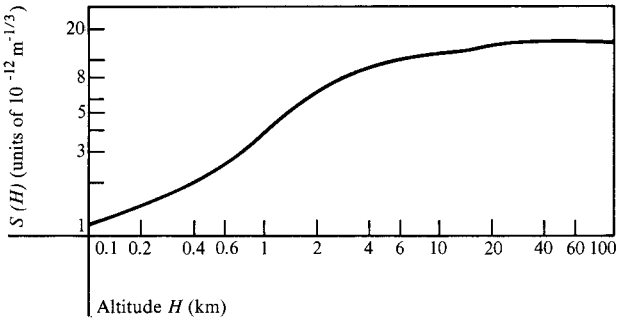

Figure 3 Empirical form integral used in the atmosphere transfer function (determined from data reported by Hufnagel and Stanley [13]).

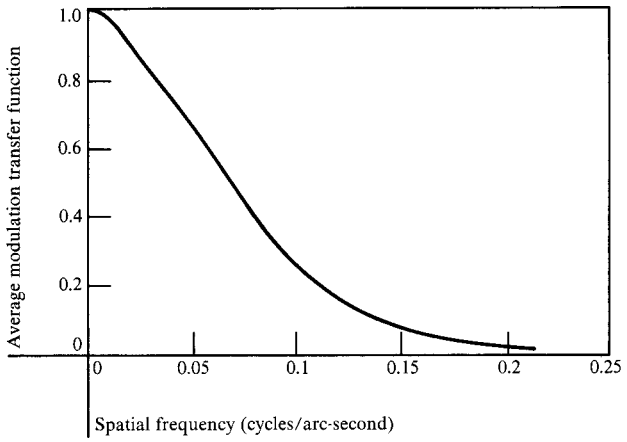

Figure 4 Atmosphere transfer function for nadir view from orbital altitude (from Hufnagel and Stanley [13]).

equation of diffusion, as discussed in a series of papers by Plass and Katawar [8]. Although a numerical solution is developed in those papers to a high degree of accuracy, computer time limitations dictate the use of approximate solutions, such as provided by Malila et al. [9] for the ultraviolet, visible and near infrared regions and by Boudreau [10] for the thermal infrared. An approximate atmospheric radiation model is sufficient for sensor system performance calculations because it is used only to estimate the magnitude of sensor incident radiance for signal-to-noise ratio calculations. The model of Malila et al. assumes a ground target located on a uniform diffuse background. Their model is used by equating the ground target to the IFOV, and the portion of test scene outside the IFOV is assumed to approximate their uniform background of reflectance equal to the average scene reflectance. This latter approximation is satisfactory for sinusoidal and square wave scenes in the range of periods of interest, but it will not hold for the step change scene; therefore, atmospheric effects are excluded in the latter case. Boudreau's thermal model assumes any one of seven models representing the temperature, pressure, and water vapor distributions. The seven models characterize a range of seasonal and local weather variations presumably encountered in remote scanning.

The polarizing effects of ground reflection and atmospheric scattering have been neglected. Their exclusion is predicated on the assumption that either a) the polarization effect is constant over the scene of interest, or b) there is no instrument polarization to interact with the incident polarized light. The former assumption is applicable to an orbital sensor whose scene of interest subtends a relatively small angle. Such is not true in the case of an airborne scanner, and the incident radiation surely exhibits variable polarization. Coulson et al. [11] have found the maximum polarization of the incident radiation to be about 20 percent, while laboratory measurements [12] of one airborne scanner have indicated an instrument polarization of about 20 percent as well. Therefore, the maximum fluctuation in sensor response created by polarization effects is about four percent and, by ignoring polarization, the present model has imposed at most that much error in the predicted response of an airborne scanner. Polarization effects merit consideration in future refinements of the model.

The scene degradation caused by atmospheric turbulence has been represented in the form of a transfer function by Hufnagel and Stanley [13]. Their normalized transfer function is

$$T_{at}(f_a) = \exp[-5.82\pi^2 \lambda^{-\frac{1}{3}} f_a^{\frac{5}{3}} S(H)/\cos\theta], \qquad (1)$$

where λ is the spectral wavelength (of band center), f_a is the spatial frequency expressed in cycles/radian, θ is the nadir angle of the ground region investigated, and $S(H)$ is an empirical form integral whose numerical value versus sensor altitude H is represented in Fig. 3. The resulting transfer function for orbital altitude ($H = 50$ km) and nadir ($\theta = 0$) is shown in Fig. 4. The function is similar to a Gaussian curve, and the point spread function exhibits a similar shape. The atmosphere transfer function is real; therefore the phase shift is zero.

• *Optics model*

The resolution properties of a diffraction-limited aberration-free lens are expressed [14] as a transfer function,

$$T_{op}(f_a) = \begin{cases} \frac{2}{\pi}[\arccos a - a(1-a^2)^{\frac{1}{2}}] & \text{for } 0 \le a \le 1 \\ 0 & \text{for } a > 1, \end{cases} \qquad (2)$$

where

$$a = f_a \lambda / D, \tag{3}$$

and D is the lens diameter. For a concave mirror, the transfer function should be modified to account for a hole or obscuration in the mirror center, a refinement not found in the present model.

The degrading effects of a focus error can be accounted for by modifying the transfer function of Eq. (2). Goodman [15] has derived a closed form expression for a square lens, and application of his technique to a circular lens yields the transfer function in integral form,

$$T_{op}(f_a) = \frac{4}{\pi} \int_0^{\frac{\pi}{2}} \frac{U \sin U + \cos U - 1}{(C \cos \psi)^2} \, d\psi, \tag{4}$$

where

$$U = C[(1 - a^2 \sin^2 \psi)^{\frac{1}{2}} - a \cos \psi] \cos \psi,$$

$$C = \pi \, (D/F)^2 \, a \, e/\lambda,$$

a is defined by Eq. (3), F is the focal length, and e is the displacement of the detector from the focal plane. Examples of the transfer function computed by Eq. (4) are illustrated in Fig. 5. The optical transfer function of either Eq. (2) or Eq. (4) is real, but the latter may be negative for certain spatial frequencies. If its sign is retained, rather than using the modulus, there is no additional phase shift function.

The primary optical element (mirror or lens) applies a geometric gain, equal to the collector area, to the incident radiance to yield the irradiance falling upon the detector in the image plane.

• *Model of the scanner-aperture interaction*

The geometry of the scanning and imaging system is described in Fig. 6. The coordinates x and y along the ground are projected normal to the line of sight, and rescaled by the ratio of focal length to altitude when projected upon the image plane. In addition, the image is rotated relative to the detector as the scanning mirror rotates or, equivalently, the detector rotates relative to the image. The image coordinates ξ and η, measured from the detector center, are related to their ground counterparts by

$$\xi = (x' - x) \, F \cos^2 \theta / H; \tag{5}$$

$$\eta = (y' - y) \, F \cos \theta / H, \tag{6}$$

where $(x' - x)$ and $(y' - y)$ are displacements from the point (x, y) marking the projection of the detector center onto the ground, and H is the altitude. The above transformation is valid because the displacements to be considered need not exceed the dimensions of the detector (i.e., the IFOV), which are very small in general, and θ is essentially constant over these dimensions. The detector, assumed rectangular in this analysis, is rotated by θ from the image coordinates ξ and η.

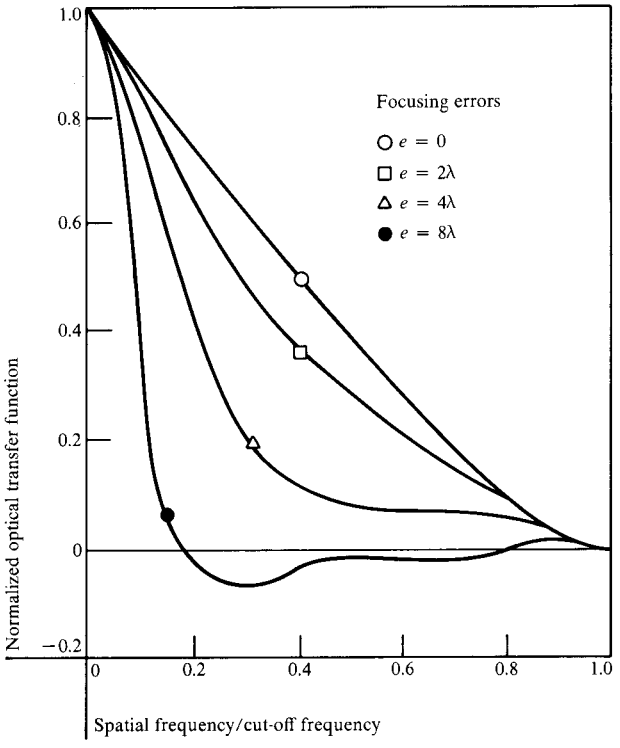

Figure 5 Optical transfer function for a circular lens with a focusing error.

The detector sums all radiation falling upon it; it therefore responds as the integral of the image radiation profile over its area in ξ, η coordinates. This integral can be written equivalently as

$$v = \int_{-\infty}^{\infty} \int_{-\infty}^{\infty} s(\xi, \eta) \, w(\xi, \eta) \, d\xi d\eta, \tag{7}$$

where $s(\xi, \eta)$ is the radiance profile in the image plane, and

$$w(\xi, \eta) = \begin{cases} 1 \text{ for } |\xi \cos \theta - \eta \sin \theta| \leq W_x/2 \text{ and} \\ \qquad |\xi \sin \theta + \eta \cos \theta| \leq W_y/2 \\ 0 \text{ elsewhere} \end{cases}$$

forces the integrand to zero outside the area of the detector dimensions W_x and W_y. Application of Eqs. (5) and (6) to Eq. (7) yields an integral over the ground coordinates,

$$v(x, y) = \int_{-\infty}^{\infty} \int_{-\infty}^{\infty} s(x', y') \, w(x', x, y', y) \, dx'dy', \tag{8}$$

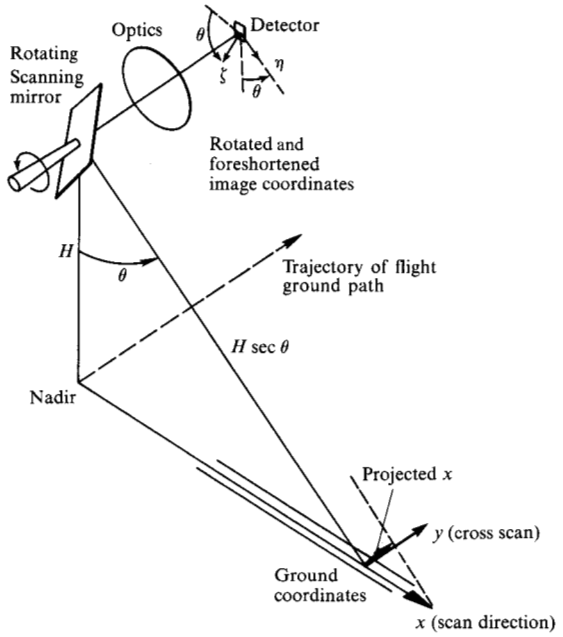

Figure 6 Geometry of the scanning and imaging system.

where

$$w(x', x, y', y)$$

$$= \begin{cases} 1 \text{ for } |(x-x')\cos^3\theta - (y-y')\cos\theta\sin\theta| \le D_x/2 \\ \quad \text{and } |(x-x')\cos^2\theta\sin\theta + (y-y')\cos^2\theta| \le D_y/2 \\ 0 \text{ elsewhere;} \end{cases}$$

$$s(x', y') = s(\xi, \eta)\ H/F\cos^3\theta$$

to account for the scale change in area, and $D_x = W_x H/F$ and $D_y = W_y H/F$ are the dimensions in the x and y directions, respectively, of the projection of the detector area upon the ground at the nadir. The integral in Eq. (8) is a convolution of the signal $s(x, y)$ with an invariant point spread function w (assuming θ constant over the region of interest); a normalized transfer function may therefore be found, namely,

$$T_{ap}(f_x, f_y) = \text{sinc } [D_x(f_x \sec\theta - f_y \tan\theta)] \times \text{sinc } [D_y\ (f_x \tan\theta \sec\theta + f_y)],$$

where f_x and f_y are the ground spatial frequencies in the x and y directions, respectively, and

$$\text{sinc } x = \sin\pi x/\pi x.$$

This investigation concentrates on ground test scenes that are spatially invariant in the downtrack (y) direction. Then, the transfer function need be considered only for $f_y = 0$, and

$$T_{ap}(f_x) = \text{sinc } (D_x f_x \sec\theta)\ \text{sinc } (D_y f_x \tan\theta \sec\theta). \quad (9)$$

The other spatial transfer functions are expressed in terms of the spatial frequency f_a measured in cycles per radian in the direction away from the line of sight. From Fig. 6, a small angular displacement α from the line of sight shown corresponds to a small linear displacement $(x' - x)$, $(y' - y)$ along the ground according to

$$\alpha = \frac{1}{H}\left[(x'-x)^2\cos^4\theta + (y'-y)^2\cos^2\theta\right]^{\frac{1}{2}}.$$

The corresponding spatial frequencies are related according to

$$f_a = H[f_x^2\sec^4\theta + f_y^2\sec^2\theta]^{\frac{1}{2}},$$

and a correspondence between the transfer functions of Eqs. (1), (2), and (9), and (11) and (12) (defined later) is established by this relation. Equation (9) may also be written

$$T_{ap}(f_a) = \text{sinc } (f_a\,\delta_x\cos\theta)\ \text{sinc } (f_a\,\delta_y\sin\theta), \quad (10)$$

where $\delta_x = D_x/H = W_x/F$ and $\delta_y = D_y/H = W_y/F$ are the angular dimensions of the IFOV.

As in the case of the optical transfer function, there is no additional phase shift function if the sign is retained in Eq. (9) or (10). The detector applies a geometric gain, equal to its area $W_x W_y$, to the incident irradiance to yield the total radiant power falling upon it.

• *Temporal frequency*

The scanning mechanism converts the spatial radiance function into a temporal function of radiance received by the detector. According to Fig. 6 the spatial coordinate x is related to the scan angle θ by $x = H\tan\theta$; therefore $dx/dt = H\sec^2\theta d\theta/dt$. Thus, assuming a constant angular rate $\dot{\theta}$, the temporal frequency f is obtained from the spatial frequency f_x by

$$f = f_x H\,\dot{\theta}\sec^2\theta.$$

The temporal response characteristics of the detector and electronics are described by a transfer function. Typically used functions with normalized moduli are [16]

$$\text{Low pass RC: } T(f) = \frac{\exp[-j\tan^{-1}(f/f_c)]}{[1+(f/f_c)^2]^{\frac{1}{2}}};$$

$$\text{High pass RC: } T(f) = \frac{f/f_c\exp[-j\tan^{-1}(f_c/f)]}{[1+(f/f_c)]^{\frac{1}{2}}};$$

$$\text{Butterworth: } T(f) = \frac{\exp[-j\phi(f)]}{[1+(f/f_c)^{2n}]^{\frac{1}{2}}};$$

$$\text{Integrate: } T(f) = \text{sinc } (f\tau);$$

where f_c is the high or low pass cutoff frequency, n is the order, $\phi(f)$ is the phase function dependent upon the implementation of the circuit, $j = \sqrt{-1}$, and τ is the integration time. The integrate transfer function is the

temporal analog of the spatial transfer function obtained earlier for an aperture.

The phase information of these transfer functions is important if the phase is not proportional to the frequency. When the phase is proportional to the frequency, there is no distortion of the signal but merely a time shift of the signal. It is to be noted that the phase function of the integrate filter is a discontinuous function of frequency, jumping from 0 to π at the zeros of the sinc function. However, if the sign is retained in the sinc function, the discontinuous phase function is accounted for automatically.

• *Nonuniform scanning rates*

The scanning rate was assumed to be a constant for the development of the relationship between the ground scene frequency and the temporal frequency. In actuality there are variations in this scanning rate. When an integrating filter is used, a transfer function can be developed to account for random variations in the motion and for high frequency periodic variations (high relative to the reciprocal of the integration time). These two effective transfer functions (derived in the Appendix) are

$$\text{Periodic: } T(f_a) = J_0(2\pi\alpha f_a); \tag{11}$$

$$\text{Random: } T(f_a) = \exp[-2(\pi\sigma f_a)^2], \tag{12}$$

where α is the amplitude of the motion in radians, J_0 is the zero-order Bessel function and σ is the standard deviation for the random angular motion in radians.

Noise contributions

Ideally, a remote sensing device detects a signal, processes it, and produces a corresponding output signal. In reality, the system receives an input information signal contaminated with noise. Each subsequent physical operation performed on the input signal introduces an additional component of noise.

A simplified model of the sensor system is defined for computing the output error as a function of the different error sources. The sensor system is assumed to have a detector, a preamplifier, and an amplifier, all operating in series. The noise generated by each unit of the system aggregate is added to the output signal of the preceding unit.

Each of the three components of the sensor system is assumed to be a linear system in itself. The input signal $x(t)$ and all the noise signals are assumed to be stationary processes in the wide sense (weakly stationary), which are also statistically independent of each other.

For a linear system, the output spectral density is the product of the input density with the square of the modulus transfer function [17]. A three-fold application of this relation to the three component system yields the output noise spectral density

$$N_0(f) = |T_a(f)|^2\{|T_p(f)|^2[|T_d(f)|^2 N_i(f) + N_d(f) + N_p(f))] + N_a(f)\},$$

where $T_{d,p,a}(f)$ are the transfer functions for the detector, preamplifier, and amplifier, respectively, $N_i(f)$ is the spectral density of the input noise, $N_{d,p,a}(f)$ are the spectral densities of the detector, preamplifier, and amplifier produced noises, respectively, and $N_0(f)$ is the spectral density of the output noise.

The noise sources, which are added by the components of the sensor, are generally the result of internally-generated thermal (Johnson) noise, as described by Papoulis [18]. The spectral characteristics for these errors are often provided in the form of a noise figure, which is the ratio of the spectral density to a thermal noise (flat spectrum) at a specified temperature and resistance. In practice, the significant error is either the detector noise (for infrared and near infrared channels) or the input noise (photon fluctuations in the visual channels); often the other noise sources can be neglected.

The input noise results from the statistical fluctuation of photons arriving at the detector and the fluctuation of electrons generated by the detector. The photon flux is modeled as a sequence of Poisson impulses. Thus, if the mean flux of photons is Φ, the variance is also Φ, and the spectral density for the photon fluctuation is flat [19].

The output current of the detector resulting from the input photon flux has the spectral density [20]

$$s_I(f) = \bar{n}|T_d(f)|^2 + (q\bar{n})^2\delta(f),\ \bar{n} = \Gamma L,\ L = \kappa h\nu\Phi,$$

where $\bar{n}$ is the average number of electrons emitted by the detector per unit time interval, L is the radiance, h is Planck's constant, ν is the optical frequency of the radiation, Γ is the photoelectric efficiency of the detector, q is the electronic charge, κ is a constant accounting for the optical system characteristics, and $\delta(f)$ is the Dirac delta function. The second term of this equation is the average current: $\bar{I} = q\bar{n}$. For frequencies low compared to the reciprocal of the electron transit time, the spectral density is approximated by

$$s_I(f) = \bar{n}|T_d(0)|^2 + \bar{I}^2\delta(f) = q\bar{I} + \bar{I}^2\delta(f),$$

where $T_d(0) = \int_{-\infty}^{\infty} h_d(t)\,dt = q$ is noted, $h_d(t)$ being the impulse response function of the detector. The spectral density of the input noise out of the detector is thus given by $E(f) = q\bar{I}$.

Some detectors, such as photomultiplier tubes, have an internal gain which has statistical variations. Experimental results are available to express the spectral density including this effect as [7]

$$E(f) = \bar{I}qMP_n,$$

where M is the internal gain and P_n is an excess noise factor. This model can also be used for other detectors such as photodiodes.

For performance calculations, the noise due to the photon fluctuation is based upon the root-mean-square value for the ground scene radiance. For example, if the ground scene radiance is a sine function, $L = A + B \sin \omega x$, where A and B are radiance values, x is the spatial coordinate, and ω is the frequency of the sine wave, then the photon fluctuation is based upon the root-mean-square value $L_{RMS} = (A^2 + \frac{1}{2}B^2)^{\frac{1}{2}}$. The total noise in the output signal to be used for computing performance parameters is obtained by integrating the output noise spectral density:

$$\sigma_0^2 = \int_{-\infty}^{\infty} N_0(f)\, df.$$

Performance calculations

The system model developed in the previous paragraphs is now used with the ground scene models described earlier to formulate both quantitative and qualitative measures of performance for the sensor system. The basic performance parameter of an imaging system is the system resolution, defined herein to be the period of a sinusoidal ground scene that corresponds to 0.5 for the modulus of the normalized overall system transfer function. A second performance parameter is the signal-to-noise ratio computed for a sinusoidal ground scene. For this calculation the signal is defined as the peak-to-peak response of the system to a sinusoidal input, and the noise is the standard deviation of the total noise out of the system. For a linear system the response to a sinusoidal input is also sinusoidal, and the peak-to-peak response is twice the response amplitude. In terms of previously defined parameters, the signal-to-noise ratio is then

$$S/N = 2A|T_{sys}(f)|/\sigma_0,$$

where A is the atmosphere-attenuated amplitude of the sinusoidal ground scene of frequency f. For this computation, the background radiance level must be as large as the sinusoidal component because the total radiance must be positive. Therefore, the signal-to-noise ratio is dependent upon both the background level and the sinusoidal term because the noise is a function of the root-mean-square value of the radiance. A quantitative parameter for describing the signal-to-noise ratio (which is a function of spatial frequency) is the noise-equivalent period. This parameter is the period of the sinusoidal ground scene that provides a signal-to-noise ratio of one.

The response of a system to a square wave ground scene is used as a qualitative performance measure. In this case the background level of the scene is not important because the measure of performance is how well the system responds to the alternating high and low levels of the scene.

A quantitative measure of the high frequency response of a system is given by the rise distance. This quantity is defined as the spatial distance over which the response signal rises from ten to 90 percent of its maximum amplitude for a step change in the ground scene.

Qualifying models with test data

In the preceding sections a model has been developed and performance parameters defined for a sensor system. The next step is the validation of the model using laboratory or flight measurement data. Flight measurements are very important in verifying the modeling of error sources for the system. Quite often additional sources of error are discovered, which arise from such items as power supplies, cooling pumps, and recording systems. These error sources are strictly periodic, or at least narrow band, and can be removed from the data, improving the appearance of a reconstructed scene. Care must be taken when removing such a noise to preserve the desired scene. Except for error sources, however, flight measurements cannot generally support detailed model verification because of the difficulty in obtaining precise "ground truth" for test targets and in eliminating atmospheric effects from the measurement data.

Laboratory measurements can be performed relatively easily to verify the system model. This is particularly true for some of the components, e.g., the response functions of the electronics and the transmission of the optical system. Additionally, the spectral density of the noise in the system can be obtained both on a component and a system basis. The total system transfer function cannot be directly obtained with laboratory measurements because of the difficulty of constructing a test target characterized by sinusoidal variation. The test target most often used is an alternating light and dark bar pattern, i.e., a square wave of finite length. For application to analyzing this type of test data, it is convenient to develop a so-called square wave transfer function by ignoring the nonlinear portion of the phase information of the system transfer function. The square wave transfer function is defined as the peak-to-peak response of the system to a square wave target normalized to zero frequency. If the argument of the system sinusoidal transfer function is proportional to the spatial frequency, an analytic expression for the square wave transfer function is obtained as follows.

The Fourier spectrum (the sequence of Fourier coefficients) of the ground square wave scene is multiplied by the system transfer function to obtain the spectrum of the system output. Because the square wave spectrum is discrete, the output spectrum is also discrete, and its Fourier transform for the system output is a Fourier series. By a judicious choice of origin, that series can be made to contain only cosine terms. Only the peak-to-peak response is desired; therefore the series is to be

evaluated only at its minimum and maximum values, viz., the two arguments at which all the cosines are ± 1, respectively. If the resulting series for the minimum and for the maximum are divided by their difference for infinite period, the result is

$$T_{sw}(f) = \frac{4}{\pi} \sum_{n=1}^{\infty} \frac{(-1)^{n+1}}{2n-1} T_{sys}[(2n-1)f],$$

where f is the number of alternating light and dark bar pairs per unit distance, i.e., the reciprocal of the square wave period; $T_{sw}(f)$ is the square wave transfer function, and $T_{sys}(f)$ is the system transfer function with a phase function proportional to frequency. In practice, $T_{sys}(f)$ vanishes at some cut-off frequency, and the series described above can be truncated without loss of accuracy.

The square wave transfer function derived above is used to compare the formulated sensor model to the RS-18B infrared radiometric scanner [21] used in the NASA Earth resources aircraft program. The assumed model includes the detector aperture, an optical system (approximated by an aberration-free lens), and an amplifier (approximated by a low-pass RC filter with linear phase shift). The transfer functions for these components were evaluated from the equations given earlier, into which the manufacturer's specifications from [21] were substituted. The resulting $T_{sw}(f)$ is compared in Fig. 10 with laboratory measurements [22] of the peak-to-peak response to several three-bar targets of different sizes used to approximate square wave scenes. Curves are given in Fig. 7 for successive incorporation of the three system components. Note the improving agreement as additional components are included in the model.

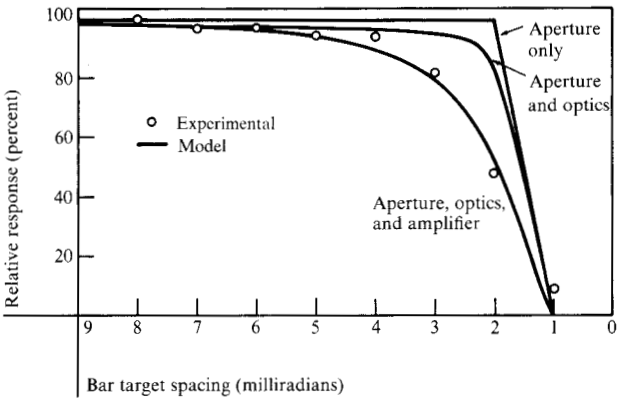

Figure 7 Normalized system response of the RS-18B infrared scanner to a three-bar target. The predicted curves are compared to laboratory measurements [22].

Summary

A mathematical model of a remote sensor system has been constructed by combining models of electronic and optical imaging systems with a model for radiative transfer in the Earth's atmosphere. In addition, the effects of certain scanning and sensor motions were included as component models. It was assumed that the sensor is a linear, invariant system and that a rather simple model of the atmosphere is adequate for system performance prediction.

Some results of the model were compared to available laboratory data for one remote sensor, and the agreement is reasonably good. That comparison is more illustrative of the technique than a validation of the model. In fact, the model must be validated for each sensor system before attempting to predict performance characteristics for that sensor. In addition to the illustrated comparison using the square wave peak-to-peak response, response profiles for square waves and step change targets can be used for validating the system response model, and the noise models can be compared with measured noise power spectral densities. After validation, the sensor model can be used with confidence to predict sensor resolution, signal-to-noise ratio, the noise equivalent ground period and radiance, the rise distance, and the square wave response of the sensor while in flight.

Acknowledgments

The authors gratefully acknowledge the assistance provided by D. A. James in the formulation of the aperture transfer function and the computation of the square wave transfer functions used for comparison with laboratory data. The assistance of W. B. Warren of TRW Systems and W. L. Hayden of Aeronutronic Ford Corporation in the general formulation of the model is also gratefully acknowledged. The work was performed in part under NASA contract NAS9-14350.

Appendix: Image motion transfer functions

Vibration and random motion of the detector and optical assemblies cause the image to move relative to the detector surface. This motion adds to the uniform motion created by the scanning mechanism. The latter motion is assumed to be much slower than the former. The scanning and the physical extent of the detector cause a point on the image to "dwell" on the detector for an effective exposure time τ. If all motions are assumed to be in the scan direction only, the detector response to the image at the nominal scan angle θ_N is

$$r(\theta_N) = \int_0^{\tau} s[\theta(t)]dt.$$

where s is the image profile, and $\theta(t)$ is the actual angle caused by the motion. If an angular velocity $\gamma(t)$ is introduced such that $\theta(t) = \theta_N + \gamma(t)$, the response becomes

$$r(\theta_N) = \int_0^{\tau} s[\theta_N + \gamma(t)]dt.$$

The Fourier transform of this equation is

$$R(f_a) = \int_0^\tau S(f_a) e^{2\pi j f_a \gamma(t)} dt,$$

where R and S are the transforms of r and s, respectively, f_a is the angular frequency, and the exponential is a phase shift caused by the displacement $\gamma(t)$; $S(f_a)$ can be removed from the integral, and the latter assumes the role of a transfer function,

$$T(f_a) = \int_0^\tau e^{2\pi j f_a \gamma(t)} dt. \qquad \text{(A1)}$$

Two types of motion are considered for evaluating $\gamma(t)$, and hence $T(f_a)$.

• *Vibration*

The vibration is assumed to be simple harmonic motion, and

$$\gamma(t) = \alpha \sin(2\pi K t + \phi),$$

where α is the angular amplitude, K is the vibration frequency and ϕ is an arbitrary phase. Substitution into Eq. (A1) yields

$$T(f_a) = (1/2\pi K) \int_\phi^{2\pi K\tau + \phi} e^{2\pi j f_a \alpha \sin\xi} d\xi, \qquad \text{(A2)}$$

where $\xi = 2\pi K t + \phi$ has been introduced for simplicity. The exponential is rewritten in terms of the corresponding sine and cosine, and the relations expressing them in Bessel functions, viz.,

$$\cos(z \sin\xi) = J_0 + 2 \sum_{n=1}^{\infty} J_{2n}(z) \cos 2n\xi;$$

$$\sin(z \sin\xi) = 2 \sum_{n=1}^{\infty} J_{2n-1}(z) \sin(2n-1)\xi,$$

are used to convert Eq. (A2) into

$$T(f_a) = (1/2\pi K) \int_\phi^{2\pi K\tau + \phi} \{J_0(2\pi\alpha f_a) + 2 \sum_{n=1}^{\infty} [J_{2n}(2\pi\alpha f_a)\cos 2n\xi + jJ_{2n-1}(2\pi\alpha f_a)\sin(2n-1)\xi]\} d\xi.$$

Integration yields

$$T(f_a) = \tau J_0(2\pi\alpha f_a) + 2 \sum_{n=1}^{\infty} \{J_{2n}(2\pi\alpha f_a) \frac{\sin 2n\pi K\tau}{2n\pi K\tau} \cos 2n(\pi K\tau + \phi) + jJ_{2n-1}(2\pi\alpha f_a) \frac{\sin(2n-1)\pi K\tau}{(2n-1)\pi K\tau} \times \sin[(2n-1)(\pi K\tau + \phi)]\}.$$

For $K\tau \gg 1$ (i.e., a vibrational period $1/K \ll \tau$), all terms vanish but the first, and

$$T(f_a) = \tau J_0(2\pi\alpha f_a).$$

This form is normalized to unity at zero frequency to obtain

$$T(f_a) = J_0(2\pi\alpha f_a),$$

which is Eq. (11).

• *Random motion*

It is assumed that during the exposure time τ the image undergoes many small motions, each of a normally distributed velocity $\gamma(t)$. Then, the effective transfer function is the expected value of the instantaneous transfer function,

$$T(f_a) = \mathrm{E}\left\{\int_0^\tau e^{2\pi j f_a \gamma(t)} dt\right\} = \int_{-\infty}^{\infty} \frac{1}{\sqrt{2\pi}\,\sigma} e^{-\gamma^2/2\sigma^2} \left[\int_0^\tau e^{2\pi j f_a \gamma(t)} dt\right] d\gamma,$$

where the factor outside the brackets is the velocity probability distribution for zero mean and standard deviation σ. Since γ is stationary, the integrals above can be interchanged, or

$$T(f_a) = \int_0^\tau dt \int_{-\infty}^{\infty} \frac{1}{\sqrt{2\pi}\,\sigma} e^{-\gamma^2/2\sigma^2} e^{2\pi j f_a \gamma} d\gamma.$$

These integrals are readily evaluated to yield

$$T(f_a) = \tau e^{-2(\pi\sigma f_a)^2},$$

or, after normalization to unity at zero frequency,

$$T(f_a) = e^{-2(\pi\sigma f_a)^2},$$

which is Eq. (12).

References

1. R. K. Holz, *The Surveillant Science—Remote Sensing of the Environment*, Houghton Mifflin, Co., Inc., Boston, 1973.
2. P. E. Johnson, editor, *Remote Sensing in Ecology*, University of Georgia Press, Athens, GA, 1969.
3. *Remote Sensing with Special Reference to Agriculture and Forestry*, National Research Council, National Academy of Sciences, Washington, D.C., 1970.
4. A. Papoulis, *The Fourier Integral and Its Applications*, McGraw-Hill Book Co., Inc., New York, 1962.
5. J. W. Goodman, *Introduction to Fourier Optics*, McGraw-Hill Book Co., Inc., New York, 1968.
6. P. Moon, "Proposed Standard Solar Radiation Curves for Engineering Use," *J. Franklin Inst.* **230,** 583 (1940).
7. H. Melchoir, M. B. Fisher, and F. P. Arams, "Photodetectors for Optical Communications Systems," *Proc. IEEE* **58,** 1466 (1970).
8. G. N. Plass and G. W. Kattawar, *Appl. Opt.* 7, 361, 415, 699, 869 (1968).
9. W. A. Malila, R. B. Crane, C. A. Omarzu, and R. E. Turner, "Studies of the Spectral Discrimination," NASA Contract NAS9-9784, May 1971, Willow Run Laboratories, U. of Michigan, Ann Arbor, MI 48107.

10. R. D. Boudreau, "A Radiation Model for Calculating Atmospheric Corrections to Remotely Sensed Infrared Measurements, Version II," NASA Earth Resources Laboratory Report 053, Mississippi Test Facility, April 1972.
11. K. L. Coulson, G. M. B. Bouricius, and E. L. Gray, "Effects of Surface Reflection on Radiation Emerging from the Top of a Planetary Atmosphere," NASA Contract NAS5-3925, December 1965, Missile and Space Division, General Electric Co.; available from the National Technical Information Service, U.S. Commerce Dept., Springfield, VA 22151.
12. P. G. Hasell et al., "Michigan Experimental Multispectral Mapping System—a Description of the M7 Airborne Sensor and Its Performance," January 1974, Infrared and Optics Division, Environmental Research Institute of Michigan, P.O. Box 618, Ann Arbor, MI 48107.
13. R. E. Hufnagel and N. R. Stanley, "Modulation Transfer Function Associated with Image Transmission through Turbulent Media," *J. Opt. Soc. America* **54**, 52 (1964).
14. Reference 5, p. 120.
15. Reference 5, pp. 123-125.
16. E. M. Grabbe, S. Ramo, and D. E. Woolridge, *Handbook of Automation, Computation, and Control*, John Wiley and Sons, Inc., New York, 1958, p. 20-15; W. R. LePage and S. Seely, *General Network Analysis*, McGraw-Hill Book Co., Inc., New York, 1952, pp. 238-256.
17. A. Papoulis, *Probability, Random Variables, and Stochastic Processes*, McGraw-Hill Book Co., Inc., New York, 1965, p. 347.
18. Ibid., p. 360.
19. Ibid., pp. 284-287.
20. W. B. Davenport, Jr. and W. L. Rood, *An Introduction to the Theory of Random Signals and Noise*, McGraw-Hill Book Co., Inc., New York, 1958, p. 123.
21. "Operations and Maintenence Manual with Parts List—RS-18B Infrared System," NASA Contract NAS9-13388, Electro-Optics Division, Texas Instruments, Inc., Dallas, TX; available from the National Technical Information Service, U.S. Dept. of Commerce, Springfield, VA 22151.
22. Informal transmittal of RS-18B laboratory data from NASA, Johnson Space Center, Houston, Texas.

Received February 16, 1975

The authors are with the IBM Federal Systems Division, 1322 Space Park Drive, Houston, Texas 77058.